RESEARCH ARTICLE

NANO · MICRO small
www.small-journal.com

Long-Acting In Situ Cancer Vaccines by Oncolytic STING-Activating Microgels

Hujing Tan, Jiakun Guo, Yan Wang, Wanting Chen, Zhiyuan Zhong, and Chao Deng**

In situ cancer vaccines exploiting endogenous multiple antigens directly from tumors to elicit broad immune responses hold great potential in cancer treatment. However, the feeble antigen presentation and hostile immune microenvironments pose severe challenges to acquiring clinical benefits. Here, oncolytic STING-activating microgels (OSAM) that release oncolytic peptide LTX-315 and STING adjuvant diABZI in a sustained manner (>4 weeks) have been developed to elicit long-acting and powerful antitumor immunity. OSAM induced significant upregulation of MHC I and substantial activation of dendritic cells for more than one week. One single intratumoral administration of OSAM markedly promoted the infiltration of cytotoxic T lymphocytes and natural killer cells, which combining with anti-CTLA-4 microgels afforded exceptional therapeutic benefits in several different murine tumor models with a cure rate of 40%–71%. These oncolytic STING-activating microgels introduce a new and powerful strategy to in situ cancer vaccines.

1. Introduction

Cancer vaccines that replenish the host with tumor-reactive T cells by improving the release, processing, and presentation of typically exogenous tumor antigens to regain control over tumor growth hold great promise for cancer treatment.[1,2] To avoid a costly and lengthy process of antigen identification, in situ cancer vaccines exploiting multiple endogenous antigens directly from tumors to elicit broad immune responses have recently gained increasing interest.[3–5] However, the feeble antigen presentation and hostile immune microenvironments pose severe challenges to acquiring clinical benefits.[6–8]

Chemotherapeutics, X-ray radiation, ablation, photothermal, and photodynamic modalities that are able to induce immunogenic cell death (ICD) and tumor-specific antigens have been explored to generate in situ cancer vaccines.[9–15] The adverse effects on normal and immune cells, however, might lead to severe adverse effects.[16,17] Besides, the feeble and short-lived immune activation leads to transient anticancer immunity even after multiple booster vaccinations. Tumor-specific antigen processing and presentation in dendritic cells can be improved by the activation of pattern recognition receptors (PRRs) such as Toll-like receptors (TLRs), nucleotide oligomerization domain-like receptors (NLRs), and stimulator of interferon genes (STING).[18–22] STING agonists that are capable of activating the STING pathway, triggering the production of type I interferons, and priming cytotoxic T lymphocytes along with natural killer cells hold great promise as adjuvants for cancer vaccines.[23–27] Despite their potential efficacy, the application of STING agonists, typically cyclic dinucleotides (CDNs), is hampered by their low stability, limited access to cytosols, strong inflammation at the site of injection, and systemic toxicity due to off-target activation.[28,29]

In this contribution, we have developed oncolytic STING-activating microgels (OSAM) that release oncolytic peptide LTX-315 and STING adjuvant diABZI in a sustained manner as an in situ cancer vaccine to elicit potent and long-acting antitumor immunity (**Scheme 1**). The microgels constructed from hyaluronic acid (HA) via microfluidic technique would afford excellent biodegradability, injectability, and uniform sizes.[30–32] Leveraging the strong ionic and hydrogen bonds between drugs and HA, OSAM would provide robust loading and controlled release of both LTX-315 and diABZI. LTX-315 is employed to induce tumor cell necrosis by disrupting the cell membrane, triggering the release of intracellular components including tumor-associated antigens and damage associated molecular patterns (DAMPs).[33–35] The antigen release enabled by LTX-315 was demonstrated in previous studies for the development of in situ tumor vaccines.[36] The released DAMPs combined with diABZI serve as adjuvants to activate the antigen presenting cells for priming adaptive tumor-specific immune responses. Thus, OSAM capable of simultaneous and continuous release of LTX-315 and diABZI within tumors would be employed as potent in situ cancer vaccines to elicit long-term antitumor immunity. Notably, a single intratumoral administration of OSAM markedly promoted the infiltration of cytotoxic T lymphocytes and natural killer cells, which combining with anti-CTLA-4-loaded microgels (C4M) afforded exceptional therapeutic benefits in several

H. Tan, J. Guo, Y. Wang, W. Chen, Z. Zhong, C. Deng
Biomedical Polymers Laboratory
and Jiangsu Key Laboratory of Advanced Functional Polymer Materials
College of Chemistry
Chemical Engineering and Materials Science
and State Key Laboratory of Radiation Medicine and Protection
Soochow University
Suzhou 215123, China
E-mail: zyzhong@suda.edu.cn; cdeng@suda.edu.cn

The ORCID identification number(s) for the author(s) of this article can be found under https://doi.org/10.1002/smll.202503561

DOI: 10.1002/smll.202503561

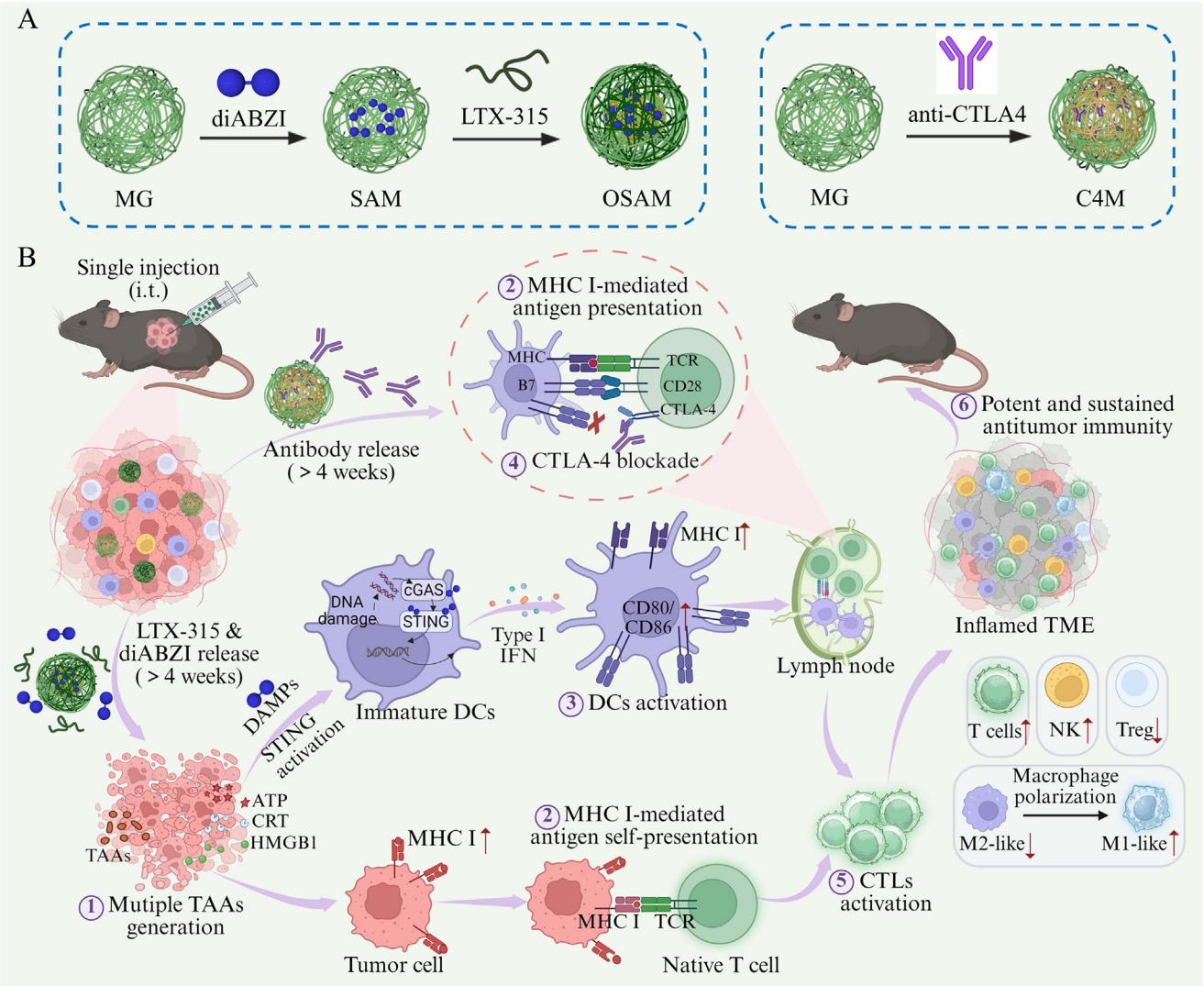

Scheme 1. Schematic illustration of oncolytic STING-activating microgels (OSAM) that release oncolytic peptide LTX-315 and STING adjuvant diABZI in a sustained manner (> 4 weeks) as an in situ cancer vaccine to elicit long-acting and powerful antitumor immunity. A) Construction of OSAM and anti-CTLA-4-loaded MG (C4M). B) OSAM elicits abundant tumor-specific antigens, upregulation of major histocompatibility complex class I (MHC I), activation of dendritic cells (DCs), immune checkpoint blockade, and infiltration of cytotoxic T lymphocytes (CTLs), leading to potent and sustained antitumor immunity.

different murine tumor models with a cure rate of 40–71%. These oncolytic STING-activating microgels open a new avenue to in situ therapeutic cancer vaccines.

2. Results and Discussion

2.1. Microgel Construction and Drug Loading

diABZI and LTX-315-loaded microgels (OSAM) were constructed through sequentially mixing diABZI and LTX-315 with microgels based on hyaluronic acid derivatives (MG). MG prepared by combining microfluidic and free radical polymerization techniques presented uniform sizes with an average diameter of 70 μm, narrow distribution (CV< 2.0%), and spherical morphology (**Figure 1A**). Unlike conventional CDNs STING agonists, diABZI bearing pyrazol and benzimidazole groups have superior in vivo stability and are positively charged, facilitating the cellular uptake to bind with STING protein.[37] Moreover, diABZI as a potent STING agonist has been employed to treat refractory/relapsed solid tumors and myeloid malignancies in clinical trials. However, the clinical application of diABZI still confronts challenges such as rapid in vivo clearance, poor tumor accumulation, and systemic toxicity due to off-target activation.[38,39] Microgels are assumed to provide robust encapsulation and persistent release of diABZI, affording safe and sustained immune stimulation. Leveraging strong electrostatic and hydrogen bonding interactions, diABZI-loaded MG (SAM) was readily constructed by mixing diABZI with MG for 30 min. When the theoretical drug loading content (DLC) ranged from 2 to 6 wt.%, diABZI exhibited efficient encapsulation with a drug loading efficiency (DLE)

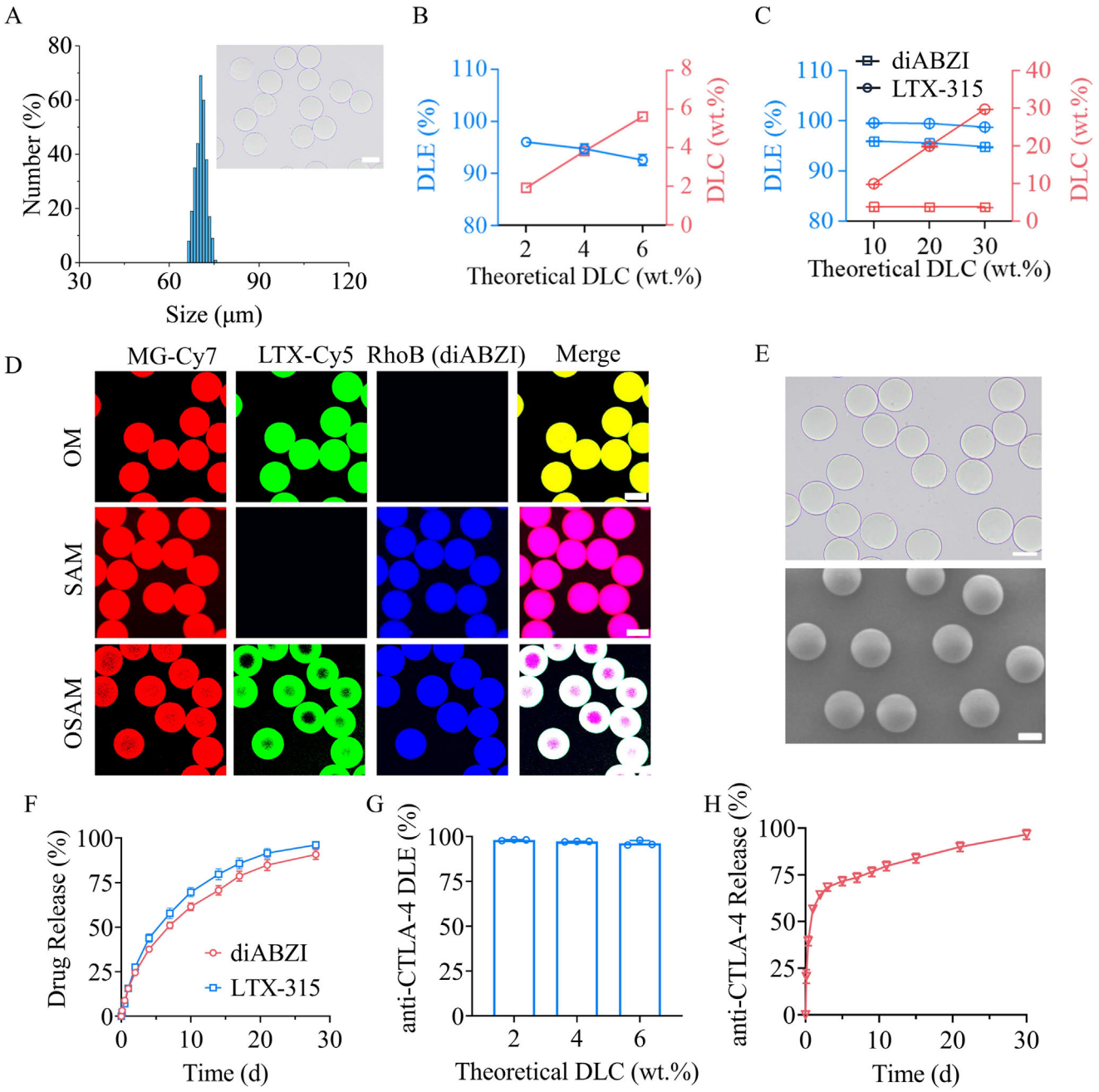

Figure 1. Construction and characterization of diABZI and LTX-315-loaded microgels (OSAM). A) Size and size distribution of blank microgels (MG) determined by microscopy (n = 300). Inset: microscopy image. B) DLE and DLC of diABZI in MG (n = 3). C) DLE and DLC of LTX-315 and diABZI (n = 3). D) Confocal laser scanning microscopy (CLSM) images of OM, SAM, and OSAM. E) Size distribution and morphology of OSAM observed by microscopy (top) and scanning electron microscopy (bottom). F) In vitro release curves of diABZI and LTX-315 from OSAM at pH 6.5 (n = 3). G) Anti-CTLA-4 loading in MG (n = 3). H) In vitro release curve of anti-CTLA-4 (n = 3). Scale bars: 50 μm.

of above 90% (Figure 1B). The diABZI loading level in SAM was further improved by LTX-315 coating, in which both diABZI and LTX-315 revealed a high DLE of ≈95% (Figure 1C). LTX-315 was labeled with fluorescent Cy5 and positively charged rhodamine B dye was used as a diABZI substitute to observe the drug loading and distribution in microgels. Confocal imaging clearly presented that rhodamine B was evenly distributed in OSAM and LTX-315 was dominantly located in the outer layer (Figure 1D). The drug loading caused little influence on the size and morphology of microgels, and OSAM displayed uniform size distribution, spherical morphology, and smooth surface (Figure 1E). In vitro drug release displayed that diABZI and LTX-315 experienced controlled and sustained release from OSAM for up to four weeks at pH 6.5 (Figure 1F). Meanwhile, anti-CTLA-4 could be similarly encapsulated in microgels (C4M) by simply mixing with a high DLE of over 95% at theoretical DLC ranging from 2% to

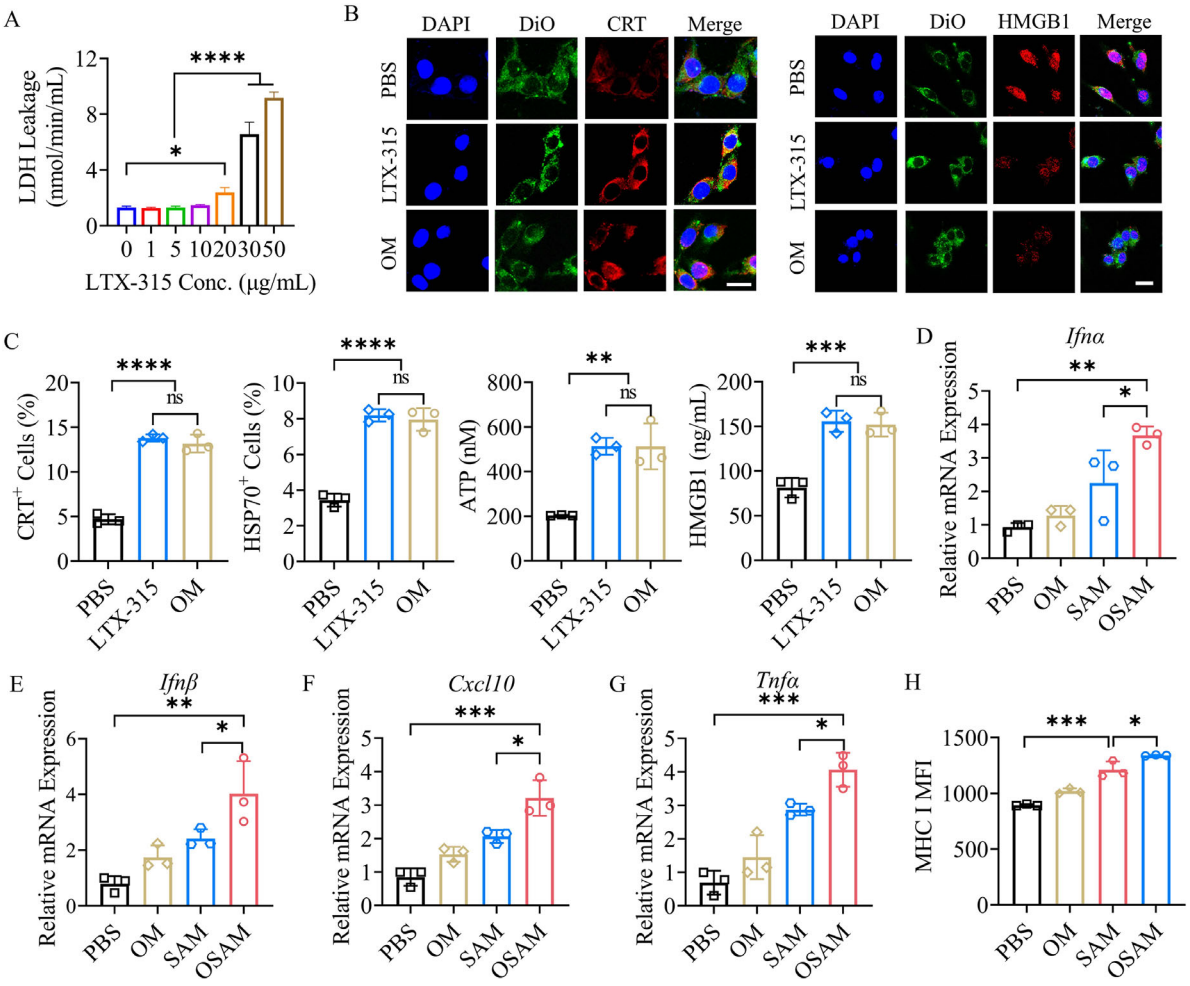

Figure 2. Evaluation of immunogenic cell death (ICD) effect and immunostimulatory capacity of OSAM in B16F10 tumor cells, $n = 3$. A) Assay of lactic acid dehydrogenase (LDH) leakage of B16F10 cells treated with oncolytic microgels (OM). B) CLSM images of B16F10 cells treated with different formulations for 24 h. Scale bars: 20 μm. The cell membrane and cell nucleus were stained with Dio and DAPI, respectively. The CRT and HMGB1 were stained with APC-labeled CRT and HMGB1 antibodies, respectively. C) Levels of ATP, HMGB1, CRT, and HSP70 in B16F10 cells after 24 h treatment. D–G) mRNA expressions of type I IFN and inflammation-related genes (*Ifnα* (D), *Ifnβ* (E), *Cxcl10* (F), and *Tnfα* (G)) in B16F10 cells after 24 h treatment measured by RT–qPCR. The results are expressed as the fold change relative to the corresponding level in PBS group. H) Mean fluorescence intensity (MFI) of MHC I on the surface of B16F10 cells treated with OSAM (40 μg mL^{-1} LTX-315 and 2 μM diABZI) for 24 h. Data are presented as mean ± SD and statistical significance was analyzed via one-way ANOVA with Tukey's multiple comparison test. p value: $^{*}p < 0.05$, $^{**}p < 0.01$, $^{***}p < 0.001$, $^{****}p < 0.0001$.

6 wt.% (Figure 1G). At pH 6.5, anti-CTLA-4 showed a sustained release from microgels for up to one month (Figure 1H). With defined sizes and morphology, near-quantitative encapsulation and durable release of various therapeutic agents (peptides, antibodies, and immunomodulators), and superb injectability, the engineered microgel systems hold significant potential for local-regional drug delivery and immunoregulation.

2.2. Immunogenic Cell Death and Immunostimulation of OSAM in B16F10 Cells

Blank MG induced little cytotoxicity with cell viability of over 95% in both L929 fibroblast and B16F10 tumor cells after 48 h incubation at a concentration up to 1.0 mg mL^{-1} (Figure S1, Supporting Information), signifying its good biocompatibility. Notably, oncolytic microgels (OM) caused high cytotoxicity with a half-maximal inhibitory concentration (IC_{50}) of 18.36 μg mL^{-1} and equivalent apoptosis to free LTX-315 peptide in B16F10 cells (Figure S2, Supporting Information). OM induced significant leakage of lactic acid dehydrogenase (LDH) (**Figure 2A**), a recognized marker of cell membrane integrity,[40] supporting the high activity of OM on membrane rupture and oncolytic performance. Tumor cells lysed by oncolytic peptides generate tumor-associated antigens (TAAs).[41] Meanwhile, co-localization analysis of CLSM images revealed that B16F10 cells treated with OM presented apparent expression of CRT on the surface and marked decrease of HMGB1 in the nucleus (Figure 2B). Quantitative analysis showed that OM caused over 2-fold higher expression of CRT and HSP70 on the cell, and also significant increase of

ATP and HMGB1 expression outside the cells (Figure 2C), suggesting that OM induced a remarkable immunogenic cell death (ICD) with substantial DAMP release. ICD has been extensively employed to activate the maturation of dendritic cells (DCs)[42–44] and release TAAs for initiating the immune response via antigen presenting cells (APCs).[45–47]

As expected, SAM significantly upregulated the expression of interferon-α (*Ifn*α), *Ifn*β related genes via activation of STING pathway with diABZI agonist, and the expression was further boosted to over 3.5 times higher by OSAM (Figure 2D,E), possibly owing to that partial DNA damage by LTX-315 was recognized and bound by cyclic guanosine monophosphate-adenosine monophosphate synthase (cGAS) in the cGAS-STING pathway. In addition, OSAM induced the highest expression of inflammation-related genes, such as C-X-C motif Chemokine Ligand 10 (*Cxcl10*), and tumor necrosis factor-α (*Tnf*α) (Figure 2F,G). Importantly, both LTX-315 and diABZI revealed a concentration-dependent upregulation of MHC I expression in B16F10 tumor cells (Figure S3, Supporting Information), and OSAM afforded significantly higher MHC I expression compared to OM and SAM (Figure 2H). It should be noted that MHC I plays a critical role for antigen presentation, and the upregulated MHC I might promote the direct antigen presentation from tumor cells to T cells, leading to subsequent T cell activation.[48–50]

2.3. Immunoactivation of OSAM in BMDCs and BMDMs

The immunoactivation effects of OSAM on bone marrow-derived dendritic cells (BMDCs) and macrophages (BMDMs) were further investigated by treating the cells with the supernatant from B16F10 cells that had been incubated with OSAM for 24 h. In BMDCs, OM, SAM, and OSAM induced striking increase of $CD80^+CD86^+$ DCs, and OSAM revealed the most potent activation effect, yielding over 11 times more mature BMDCs compared to PBS group (**Figure 3**A,B). Besides, BMDCs treated with OSAM exhibited over 2-fold increase in MHC I expression (Figure 3C), which in combination with the substantially increased mature BMDCs would largely facilitate the delivery of tumor antigens from DCs to T cells. Notably, OSAM and free drug combination (OSA) although exhibited comparable efficacy in promoting BMDC maturation within 24 h (Figure S4, Supporting Information), OSAM capable of sustained release of LTX-315 and diABZI afforded significantly extended DC activation for over 7 days (Figure 3D,E). Compared to PBS group, OSAM elicited significantly higher mRNA expression of *Ifn*β (>10 fold), *Cxcl10* (>35 fold), *Il6* (>13 fold), *Ifn*α, and *Tnf*α genes (Figure 3F–H; Figure S5, Supporting Information), verifying the potential to improve the immune microenvironments and recruitment of immune cells. In consistent, BMDCs treated with OM, SAM, and OSAM exhibited significantly improved levels of immunostimulatory factors IL-6, TNF-α, and IL-12p70 in the supernatant, with OSAM yielding the highest concentration (Figure 3I–K). Remarkably, BMDMs treated with SAM and OSAM significantly increased the percentage of M1-like macrophages from 13.8% to 56.3% and 60.9% (Figure 3L; Figure S6, Supporting Information), respectively. In addition, OSAM afforded the highest M1/M2 ratio of 1.5, which was comparable to OSA control while ≈6-fold higher than PBS group (Figure 3M; Figure S7, Supporting Information), signifying the substantial polarization of macrophages induced by OSAM.

2.4. In Vivo Antitumor Efficacy and Immune Regulation of OSAM

The biodistribution profile of microgel formulations was initially explored in B16F10 tumor-bearing mice following intratumoral administration using an in vivo imaging system (IVIS). To facilitate real-time observation, LTX-315 and anti-CTLA-4 were labeled with Cy7 fluorophores, while RhoB was used as a fluorescent surrogate for diABZI. In contrast with the rapid clearance of free drugs (Cy7-LTX-315 and RhoB) from tumor sites with ≈30% retention at one day post-injection, OSAM demonstrated significantly prolonged drug retention, maintaining ≈73% of both drugs within tumors at one day and detectable drug even after 10 days (Figure S8, Supporting Information). The sustained retention pattern was similarly observed for antibody therapeutics, where C4M showed over 80% and 18% tumor retention of anti-CTLA-4 at one day and ten days post-administration, respectively, in sharp contrast with almost complete elimination for free antibody within 2 days (Figure S9, Supporting Information).

The in vivo antitumor efficacy was assessed in immunosuppressive "cold" B16F10 melanoma subcutaneous model (**Figure 4**A). Figure 4B shows that all MG-based formulations following intratumoral administration displayed a gradual increase in body weight of mice over time, suggesting that they possess decent safety. On the contrary, free drug combinations (OSA, OSA/C4) induced marked body weight loss, consistent with previous findings that direct injection of free LTX-315 or STING agonists frequently caused severe adverse reactions.[51,52] In sharp contrast to swift tumor growth in PBS group, a single intratumoral injection of OM, SAM, or OSAM displayed significant suppression of tumor growth, affording superior therapeutic efficacy compared to their free drug counterparts (Figure 4C,D; Figure S10, Supporting Information). In particular, mice treated with OSAM showed remarkable tumor regression with a median survival time (MST) extended to 37 days and 3 out of 7 mice complete tumor remission within 90 days. OSAM combining with C4M (OSAM/C4M) further improved the therapeutic outcomes, leading to a cure rate of 71% (Figure 4E), suggesting a potent and long-lasting antitumor immunity.

Tumor and immune cells were collected 7 days after i.t. administration of different formulations for subsequent immune response evaluation (Figure 4F). The flow cytometry measurement showed that OSAM significantly upregulated the expression of MHC I in both tumor and DCs (Figure 4G,H) and promoted the mature of DCs ($CD11c^+CD80^+CD86^+$) in lymph nodes (LNs) (Figure 4I). In addition, the number of mDCs induced by OSAM/C4M was 4.2 times higher than that in the PBS group. Notably, OSAM prominently increased the fractions of $CD8^+$ and $CD4^+$ T cells in both tumors and spleens (Figure 4J,K; Figure S11, Supporting Information), signifying the generation of robust antitumor immunity within the tumor and the system. The cell proportions were further improved by the introduction of C4M (OSAM/C4M) through the inhibition of CTLA-4 immune checkpoint on the T cells. Moreover, OSAM markedly promoted the expression of activation markers (CD69) and proliferation

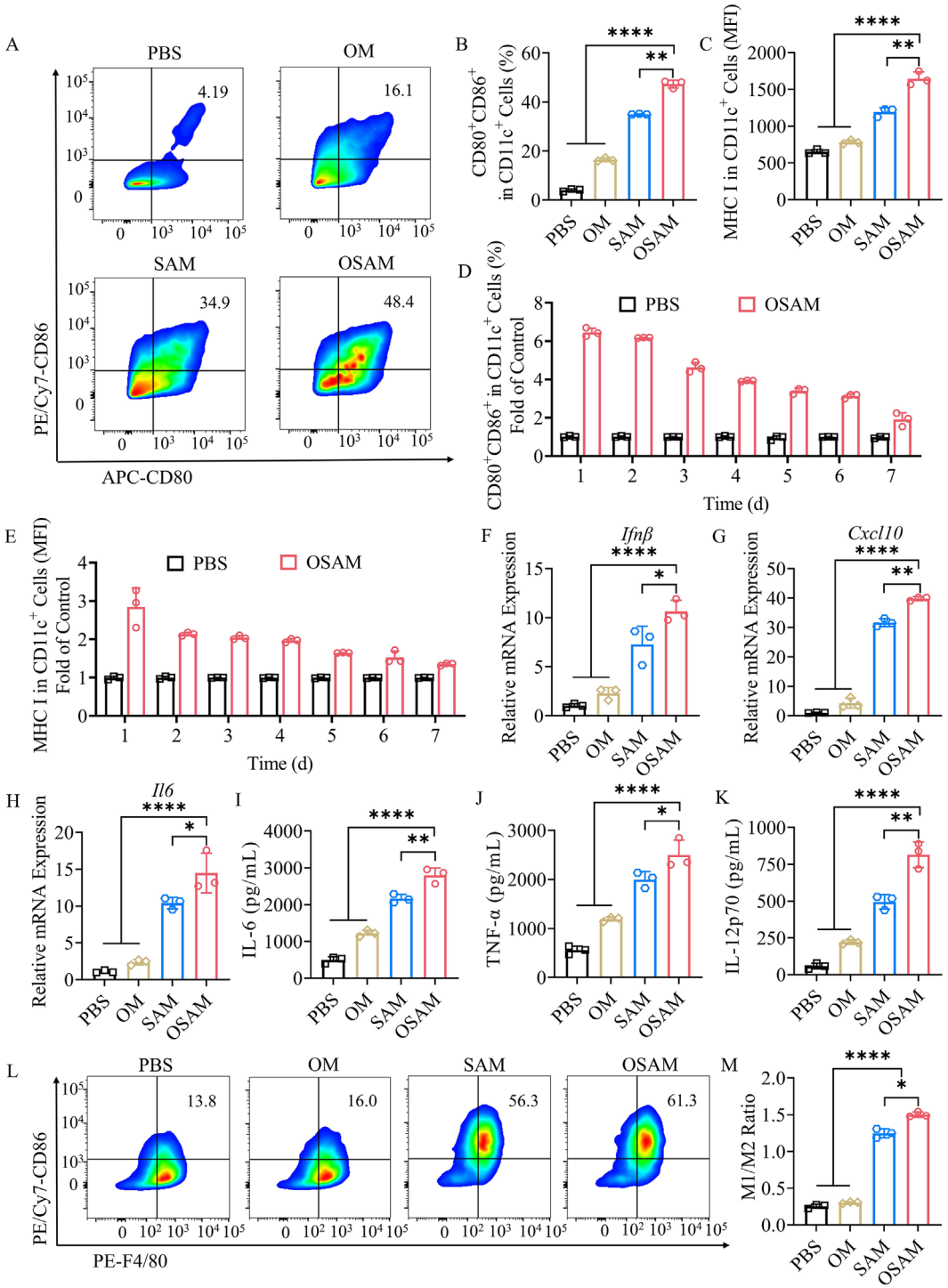

Figure 3. Immunoactivation effects of OSAM on bone marrow-derived dendritic cells (BMDCs) and macrophages (BMDMs). B16F10 cells were treated with OSAM for 24 h, and then the supernatant was added into BMDCs or BMDMs for another 24 h incubation, $n = 3$. A) Representative flow cytometry graphs of $CD80^+CD86^+$ cells in BMDCs. B) Quantification of $CD80^+CD86^+$ cells in $CD11c^+$ cells. C) MFI of MHC I in $CD11c^+$ cells. D) Quantification of $CD80^+CD86^+$ cells and E) MFI of MHC I in BMDCs. B16F10 cells were treated with OSAM for 24 h on days 1 through 7, and then the supernatant was added into BMDCs for another 24 h incubation. The results are expressed as the fold change relative to the corresponding level in the PBS group. F–H) mRNA expressions of type I IFN and inflammation-related genes (*Ifnβ* (F), *Cxcl10* (G), *Il6* (H)) in BMDCs after 24 h treatment measured by RT–qPCR. The results are expressed as the fold change relative to the corresponding level in the untreated control group. I–K) Cytokine expression of IL-6 (I), TNF-α (J), and IL-12p70 (K) in BMDCs. (L) Representative flow cytometry graphs of $F4/80^+CD86^+$ cells in BMDMs. (M) Quantification of M1/M2 ratios. Data are presented as mean ± SD and statistical significance was analyzed via one-way ANOVA with Tukey's multiple comparison test. *p* value: $^*p < 0.05$, $^{**}p < 0.01$, $^{****}p < 0.0001$.

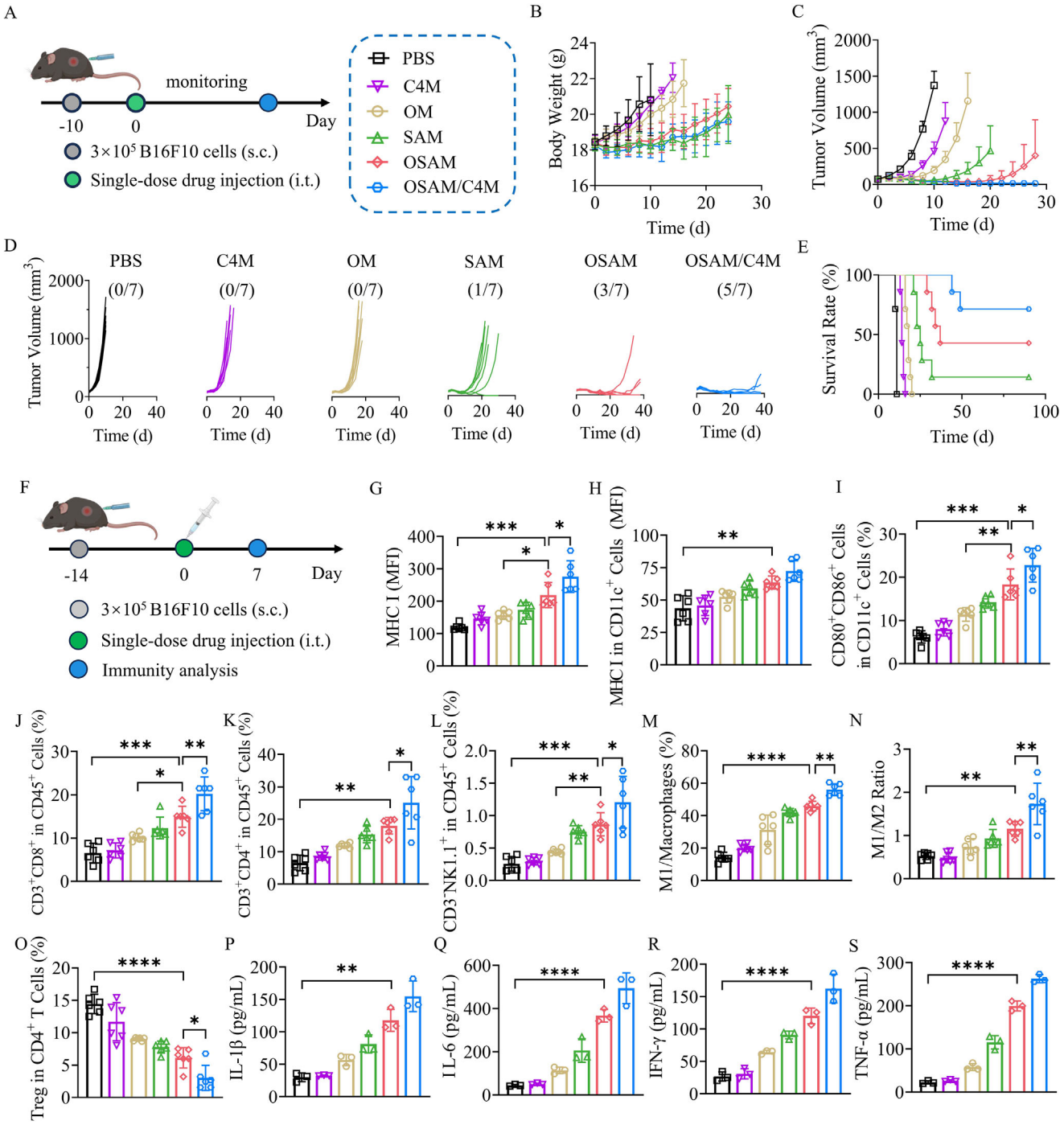

Figure 4. Antitumor efficacy and immune regulation of OSAM in subcutaneous B16F10 melanoma model. A) Schematic diagram of the establishment, treatment, and monitoring of B16F10 melanoma model. B) Body weight. C) Average tumor growth curves. D) Individual tumor growth curves. E) Survival curves. (B–E, $n = 7$). F) Schematic diagram of the establishment, treatment, and immunity analysis of B16F10 melanoma models. G) MFI of MHC I in tumor cells. H) Matured DCs ($CD80^+CD86^+CD11c^+$) in the lymph nodes. I) MFI of MHC I in DCs in the lymph nodes. J) $CD8^+$ T cells, K) $CD4^+$ T cells, L) $NK1.1^+$ cells, M) M1 macrophages ($F4/80^+CD86^+$), N) M1/M2 ratio, and O) Treg cells ($CD4^+CD25^+FoxP3^+$) in the tumors. P–S) Expression levels of proinflammatory factors including IL-1β (P), IL-6 (Q), IFN-γ (R), and TNF-α (S) in the tumor lysates analyzed by ELISA. (G–S, $n = 6$; P–S, $n = 3$). Data are presented as mean ± SD and statistical significance was analyzed via one-way ANOVA with Tukey's multiple comparison test. p value: $^{*}p < 0.05$, $^{**}p < 0.01$, $^{***}p < 0.001$, $^{****}p < 0.0001$.

markers (Ki-67) on $CD8^+$ T cells, which was further amplified when combined with C4M (Figure S12A,B, Supporting Information). Importantly, although both OM and OSAM upregulated CTLA-4 expression in $CD8^+$ T cells, the suppressive effect was reversed upon combination with C4M, thereby restoring cytotoxic T cell functionality (Figure S12C, Supporting Information). Of note, SAM and OSAM led to an over 3-fold increase in the fractions of NK1.1-positive NK cells (Figure 4L), mainly owing to the secretion of type I IFN generated by the activation of STING pathway. The infiltration of NK cells providing innate immunity has been reported to largely boost the potency of the in situ vaccine.[53,54] Meanwhile, OSAM significantly decreased the proportion of M2-TAMs ($CD45^+CD11b^+F4/80^+CD206^+$), increased the proportion of M1-TAMs ($CD45^+CD11b^+F4/80^+CD86^+$) and the ratio of M1/M2 (Figure 4M,N; Figure S13, Supporting Information), confirming the efficient macrophage polarization. Besides, a marked decline in regulatory T cells (Treg) was observed in the OSAM treated mice compared to the PBS treated mice (Figure 4O). Furthermore, the concentrations of IL-1β, IL-6, IFN-γ, and TNF-α in the tumor lysates of mice treated with OSAM were significantly increased (Figure 4P–S), indicating an effective improvement in the tumor immunosuppressive microenvironment. Importantly, although a slight elevation of proinflammatory cytokines in the serum was induced by OSAM (Figure S14, Supporting Information), the cytokine levels remained within physiologically normal ranges and were comparable to those in the nanodrug systems with established biocompatibility.[55,56] H&E staining further demonstrated preserved tissue architecture without detectable inflammatory infiltrates in major organs (heart, liver, spleen, lung, and kidney) (Figure S15, Supporting Information), indicating OSAM possessed favorable biosafety with negligible induction of inflammatory toxicity and damage to normal tissues.

Then, we evaluated the immunotherapeutic performance of OSAM in an immunosuppressive "cold" 4T1 subcutaneous tumor model (**Figure 5**A). Compared to the PBS group, OSAM and OSAM/C4M treatment significantly delayed tumor growth, extending MST from 18 d to 38 and 52 d, respectively (Figure 5B,C). In addition, 3 out of 7 mice treated with OSAM/C4M became tumor-free within 90 d. OSAM/C4M induced ≈2-fold increase of $CD8^+$ T and $CD4^+$ T cells in peripheral blood (PB) (Figure 5D–F).

4T1 bilateral tumor model was established by inoculating 4T1 tumor cells on the right (primary tumor) and left (distant tumor) sides on days −10 and −3, respectively, to assess the therapeutic effect (Figure 5G). Both OSAM and OSAM/C4M exhibited remarkable suppression on primary and distant tumors (Figure 5H,I), and induced little body weight change (Figure S16, Supporting Information). Of note, OSAM/C4M treatment induced more than 15- and 3.5-fold increases of the infiltration of cytotoxic T lymphocytes ($CD3^+CD8^+$) and $CD3^+CD4^+$ T cells in primary and distant tumors, respectively (Figure 5J,K; Figure S17A,B, Supporting Information). Also, significant upregulation of $CD8^+$ and $CD4^+$ T cells was observed in spleen, LNs, and PB (Figure 5L–N; Figure S17C–E, Supporting Information), verifying the induction of the systemic anti-tumor immunity. Therefore, intratumoral administration of OSAM demonstrates remarkable therapeutic efficacy with minimal off-target toxicity, representing a promising strategy for the treatment of various malignant tumors such as breast cancer and melanoma. Nevertheless, imaging or surgical assistance might be required for performing precise intratumoral delivery in many tumors,[57] compromising the practical applications and broader clinical translation.

2.5. Tumor Rechallenge and Anti-Tumor Immune Memory

Encouraged by the superb antitumor efficacy of OSAM and OSAM/C4M, we then assessed the immune memory by rechallenge cured mice with B16F10 melanoma cells on day 120, using healthy mice transplanted with tumor cells serving as a control group (**Figure 6**A). In contrast with fast tumor growth in control group, the cured mice presented delayed tumor progression (Figure 6B), which was further verified by the minimal increase of tumor weight on day 18 (Figure 6C). Furthermore, OSAM and OSAM/C4M effectively reversed spleen enlargement in B16F10 tumor-bearing mice (Figure 6D), indicating a reduction of systemic inflammation to the normal range,[58] which was critical to ensure safe drug administration. In addition, mice treated with OSAM and OSAM/C4M generated much more $CD8^+$ effector memory T cells (T_{EM}, $CD44^+CD62L^-$) and $CD8^+$ central memory T cells (T_{CM}, $CD44^+CD62L^+$) in both the peripheral blood (PB) and the spleen (Figure 6E–J). For example, OSAM and OSAM/C4M induced around a 3-fold increase of T_{EM} in PB compared to PBS group, resulting in strong immune memory.

The therapeutic performance of OSAM/C4M was further evaluated in the "hot" MC38 colon carcinoma model (Figure 6K), a cancer characterized by clinically significant mutations and high aggressiveness.[59,60] Notably, OSAM/C4M treatment significantly delayed tumor growth, achieving a 40% cure rate with no recurrence observed within 90 days (Figure 6L–O). Reintroducing MC38 tumor cells into cured mice on day 150 resulted in no tumor growth and complete survival (Figure 6P,Q), verifying the elicitation of a strong and long-lasting immune response.

3. Conclusion

We have developed oncolytic STING-activating microgels (OSAM) as an in situ cancer vaccine to elicit long-acting and powerful antitumor immunity. OSAM possesses several unique features: i) quantitative encapsulation and gradual release of the oncolytic peptide LTX-315 and STING adjuvant diABZI for over 4 weeks; ii) upregulation of MHC I in cancer cells to promote the self-presentation of tumor-specific antigens; iii) continuous activation of BMDCs and substantial upregulation of MHC I in BMDCs to improve antigen presentation capacity; iv) one single intratumoral administration of OSAM promoted the infiltration of cytotoxic T lymphocytes and natural killer cells to simultaneously boost innate and adaptive immunity; v) combining with anti-CTLA-4 microgels afforded exceptional therapeutic efficacy in several different murine

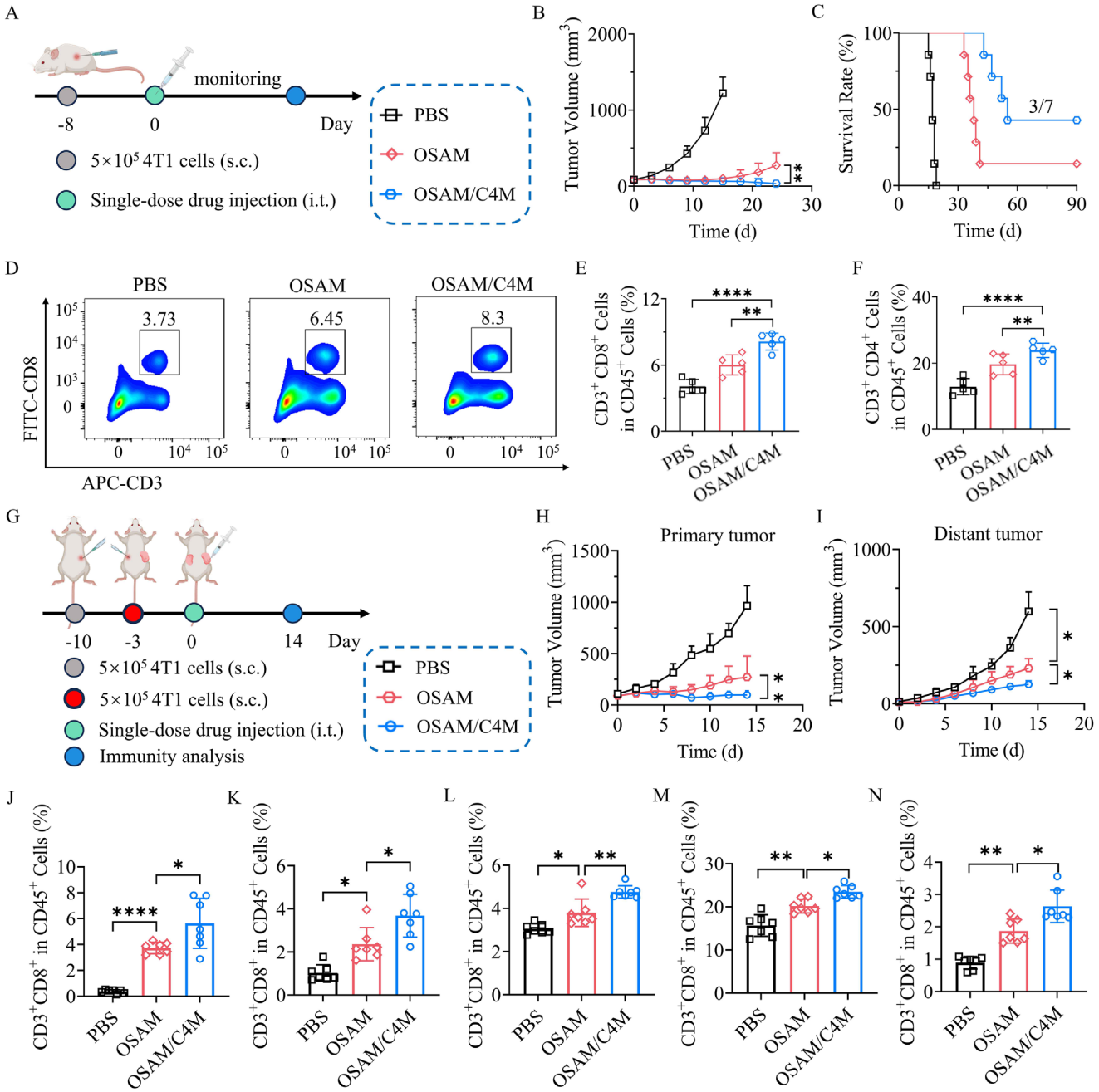

Figure 5. Antitumor efficacy and immune regulation of OSAM in subcutaneous 4T1 breast tumor model. A) Schematic diagram for the establishment, treatment, and monitoring of the 4T1 mouse model. B) Tumor growth curves. C) Survival curves. (B–C, $n = 7$). D) Representative flow cytometry graphs of $CD3^+CD8^+$ T cells in PB. E) Quantitative analysis of $CD8^+$ T cells in PB. (F) Quantitative analysis of $CD4^+$ T cells in PB. (E–F, $n = 5$). G) Schematic diagram of establishment, treatment, and monitoring of the 4T1 mouse bilateral tumor model. H) Primary tumor growth curves. I) Distant tumor growth curves. J–N) Quantitative analysis of $CD8^+$ T cells in the primary tumor (J), distant tumor (K), spleen (L), lymph nodes (M), and PB (N). H–N, $n = 7$. Data are presented as mean ± SD and statistical significance was analyzed via one-way ANOVA with Tukey's multiple comparison test. p value: $^*p < 0.05$, $^{**}p < 0.01$, $^{***}p < 0.001$, $^{****}p < 0.0001$.

tumor models with a cure rate of 40%–71%. These oncolytic STING-activating microgels represent an advanced strategy to continuously boost antigen presentation and improve immunosuppressive tumor microenvironments, providing persistent and powerful in situ therapeutic cancer vaccines.

4. Experimental Section

Loading of diABZI, LTX-315 and Anti-CTLA-4: diABZI was encapsulated in MG by simply mixing diABZI with MG in aqueous solution to obtain SAM. Briefly, an MG suspension (25 mg mL^{-1}) was mixed with an equivalent volume of diABZI solution at theoretical DLC of 2 wt.%–6 wt.%.

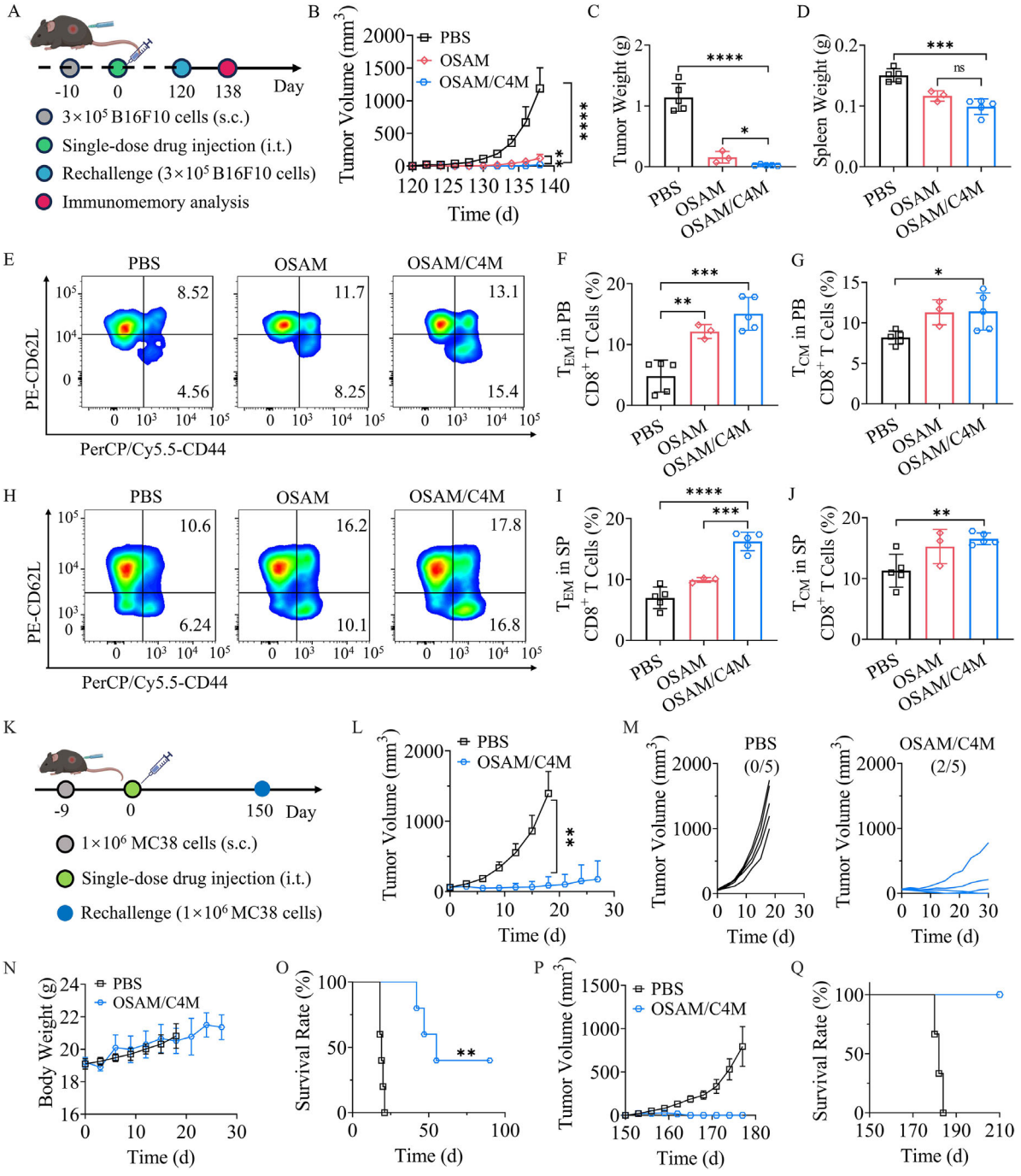

Figure 6. Tumor rechallenge and anti-tumor immune memory. A) Schematic diagram of the rechallenge and immunomemory analysis of B16F10 melanoma model. B) Tumor growth curves (PBS and OSAM/C4M: $n = 5$; OSAM: $n = 3$). C) Tumor weight. D) Spleen weight. E) Representative flow cytometry graphs of T_{EM} cells ($CD44^+CD62L^-$) and T_{CM} cells ($CD44^+CD62L^+$) among $CD3^+CD8^+$ T cells in PB on day 18 post-rechallenge. (F) Quantitative analysis of T_{EM} cells in $CD3^+CD8^+$ T cells in PB. G) Quantitative analysis of T_{CM} cells in $CD3^+CD8^+$ T cells in PB. H) Representative flow cytometry graphs of T_{EM} cells ($CD44^+CD62L^-$) and T_{CM} cells ($CD44^+CD62L^+$) among $CD3^+CD8^+$ T cells in spleen on day 18 post-rechallenge. I) Quantitative analysis of T_{EM} cells in $CD3^+CD8^+$ T cells in spleen. J) Quantitative analysis of T_{CM} cells in $CD3^+CD8^+$ T cells in spleen. K) Schematic diagram of the establishment, treatment, and rechallenge of MC38 colorectal tumor model. L) Tumor growth curves ($n = 5$). M) Individual tumor growth curves. N) Weight curves. O) Survival curves. P) Tumor growth curves following the rechallenge with MC38 cells. Q) Survival curves (Control: $n = 3$; OSAM/C4M: $n = 2$). Data are presented as mean ± SD and statistical significance was analyzed via one-way ANOVA with Tukey's multiple comparison test. p value: $^*p < 0.05$, $^{**}p < 0.01$, $^{***}p < 0.001$, $^{****}p < 0.0001$.

At predetermined time points, the unloaded diABZI in the supernatant was measured via high pressure liquid chromatography (HPLC). The drug loading efficiency (DLE) and drug loading content (DLC) were calculated according to the following formulations.

$$\text{DLE (\%)} = \text{Weight of drug loaded/Total weight of feed drug} \times 100 \quad (1)$$

$$\text{DLC (wt.\%)} = \text{Weight of drug loaded/Weight of drug and dried microgels} \times 100 \quad (2)$$

LTX-315 was encapsulated in MG by simply mixing LTX-315 with MG in aqueous solution to obtain OM. Briefly, a MG suspension (25 mg mL^{-1}) was mixed with an equivalent volume of LTX-315 solution at theoretical DLC of 10 wt.%–30 wt.%. At predetermined time points, the unloaded LTX-315 in the supernatant was measured via an ultraviolet spectrophotometer. DLE and DLC of LTX-315 were similarly calculated. OSAM was similarly prepared by mixing SAM with LTX-315.

Anti-CTLA-4 was encapsulated into MG by dialysis replacement. To 25 mg mL^{-1} of MG was added anti-CTLA-4 in PBS solution (pH 7.4, 10 mM) at theoretical loading contents of 2 wt.%–6 wt.%. Then, the mixture was dialyzed six times using a phosphate buffer (PB) solution (pH 5.0). The dialysis medium was refreshed every hour. The anti-CTLA-4-loaded MG suspension was then mixed with tannic acid (2 mg mL^{-1}) to stabilize the antibody loading. The unloaded anti-CTLA-4 in supernatant solution was detected using bicinchoninic acid (BCA) protein assay kit. DLE and DLC of anti-CTLA-4 were similarly calculated.

To evaluate drug distribution in MG, positively charged rhodamine B dye was used as a diABZI substitution, and MG and LTX-315 were labeled with Cy7 and Cy5, respectively. The OSAM solution added on the glass slide was covered with a coverslip, followed by the observation using confocal laser scanning microscopy (CLSM).

In Vitro Drug Release of diABZI, LTX-315, and Anti-CTLA-4: In vitro release of diABZI and LTX-315 from OSAM was carried out in PBS (pH 6.5, 10 mM). Briefly, 100 µL of OSAM (25 mg mL^{-1} MG) was placed in the insert of transwell plates. Then, 1.0 mL of PBS was added to the plates to immerse OSAM. The plates were placed on a shaking table at 37 °C and 100 rpm. At predetermined time points, the release medium was collected and refreshed with PBS (1.0 mL). The amount of diABZI and LTX-315 in the release medium was measured with high pressure liquid chromatography and UV spectrophotometer, respectively. In vitro release of Cy3-labeled anti-CTLA-4 from anti-CTLA-4@MG was carried out in PBS (pH 6.5, 10 mM). The antibody amount in the release medium was measured with a multifunctional microplate reader.

In Vitro Expression of MHC I: After inoculating in 6-well plates for 12 h, B16F10 cells (2×10^5) were treated with PBS, OM, SAM, or OSAM for 24 h. Then, the cells were collected and stained with anti-H-2Kb/H-2Db-PE (clone: 28-8-6) antibody, and the mean fluorescence intensity corresponding to MHC I expression was analyzed by flow cytometry.

In Vitro DC Activation: All animal experiments were approved by the Animal Care and Use Committee of Soochow University, and all protocols of animal studies conformed to the Guide for the Care and Use of Laboratory Animals (202303A0879). Bone marrow-derived dendritic cells (BMDCs) were extracted from the leg bones of healthy female C57BL/6J mice to investigate the in vitro activation of dendritic cells (DCs). B16F10 cells (2×10^5) were treated with PBS, OM, SAM, or OSAM (diABZI: 1 µM, LTX-315: 20 µg mL^{-1}) for 24 h, and then the supernatant was added to BMDCs cells seeded in 12-well plate (2×10^6/well). After 24 h incubation, the immune cells were collected, blocked on ice with anti-mouse CD16/32 for 30 min, and then incubated with anti-CD11c-FITC, anti-CD80-APC (clone: 16-10A1), anti-CD86-PE-Cy7 (clone: 53-6.7) and anti-H-2Kb/H-2Db-PE (clone: 28-8-6) antibodies for 30 min. After washing with PBS, the proportion of mature BMDCs ($CD11c^+CD80^+CD86^+$, MHC I) was assessed using flow cytometry. The culture medium was harvested for the detection of the cytokines including IL-6, TNF-α, and IL-12p70 by ELISA.

To investigate the sustained stimulation of BMDCs by OSAM, B16F10 cells (2×10^5) were inoculated into the lower chamber of Transwell plate for 12 h and then treated with OSAM loaded in the upper chamber for 24 h. The OSAM in the upper compartment of the Transwell plate was then transferred to a fresh Transwell plate pre-inoculated with B16F10 cells (2×10^5), and the supernatant was added to the BMDCs inoculated with the 12-well plate (2×10^6). After incubation for 24 h, the immune cells were collected and stained. This process was repeated for 7 times to investigate the long-term immunostimulation of OSAM in BMDCs.

In Vivo Tumor Therapy: The in vivo antitumor effects of different formulations were evaluated in subcutaneous B16F10, MC38, and 4T1 models. When the tumor volume was ≈75 mm^3, a single i.t. administration (50 µL) of different formulations (LTX-315: 45 mg kg^{-1}; diABZI: 2 mg kg^{-1}; anti-CTLA-4: 2 mg kg^{-1}) was administered on day 0. The tumor volume was measured and calculated as follows: tumor volume = $width^2 \times length \times 0.5$. The weights of the mice were recorded every other day. Mice were considered to have reached the endpoint of the study if they died, lost more than 15% of their initial body weight, or if the tumor volume reached 1500 mm^3 during treatment.

To assess immune memory, cured mice received a secondary injection of tumor cells (B16F10: 3.0×10^5; MC38: 1.0×10^6) in the left flank. Tumor volume and body weight of the mice were measured every 3 days during the experiment. Upon tumor volume reaching 1500 mm^3 in the control group, all mice were euthanized, and the peripheral blood and spleen were collected for the analysis of memory T cell phenotypes.

Immune Analysis of B16F10 and 4T1 Models: Following treatment, the tumors, spleens, and lymph nodes were harvested and ground to obtain single cell suspensions. Then, the cells were stained with corresponding antibodies (Biolegend): anti-CD45-PerCP/Cy5.5 (clone: 30-F11), anti-CD45-APC (clone: 30-F11), anti-CD3-FITC (clone: 17A2), anti-CD8-PE/Cy7 (clone: 53-6.7), anti-CD4-PE (clone: GK1.5), anti-NK1.1-PerCP/Cy5.5 (clone: PK136), anti-CD80-APC (clone: 16-10A1), anti-CD86-PE/Cy7 (clone: GL-1), anti-CD11b-FITC (clone: M1/70), anti-CD11c-FITC (clone: N418), anti-CD206-APC (clone: C068C2), anti-F4/80-PE (clone: BM8), anti-Foxp3-AF647 (clone: 150D), anti-CD25-PE/Cy7 (clone: PC61), and anti-H-2Kb/H-2Db-PE (clone: 28-8-6). Flow cytometric analysis was then performed.

Statistical Analysis: All the experimental data were statistically analyzed, and the results were expressed as a mean ± standard deviation (SD), $n \geq 3$. GraphPad Prism (version number: 9.0) software was used for statistical analysis. Statistical significance was calculated via a two-tailed Student's t-test for two-group comparisons. Statistical differences were determined using one-way two-sided analysis of variance (ANOVA) for multiple comparisons. Statistical significance was set as follows: $^*p < 0.05$, $^{**}p < 0.01$, $^{***}p < 0.001$, $^{****}p < 0.0001$, and ns denotes no significant difference.

Supporting Information

Supporting Information is available from the Wiley Online Library or from the author.

Acknowledgements

H.T. and J.G. contributed equally to this work. This work was financially supported by the National Key R&D Program of China (2021YFB3800900) and the National Natural Science Foundation of China (NSFC 52373299 and NSFC 51973149).

Conflict of Interest

The authors declare no conflict of interest.

Data Availability Statement

The data that support the findings of this study are available from the corresponding author upon reasonable request.

Keywords

cancer immunotherapy, in situ vaccine, microparticles, oncolytic peptide, STING

Received: March 19, 2025
Revised: July 19, 2025
Published online: August 5, 2025

[1] M. Saxena, S. H. van der Burg, C. J. M. Melief, N. Bhardwaj, *Nat. Rev. Cancer* **2021**, *21*, 360.
[2] M. C. Sellars, C. J. Wu, E. F. Fritsch, *Cell* **2022**, *185*, 2770.
[3] N. Gong, M.-G. Alameh, R. El-Mayta, L. Xue, D. Weissman, M. J. Mitchell, *Nat. Rev. Drug Discovery* **2024**, *23*, 607.
[4] Y. Zhang, S. Ma, X. Liu, Y. Xu, J. Zhao, X. Si, H. Li, Z. Huang, Z. Wang, Z. Tang, W. Song, X. Chen, *Adv. Mater.* **2021**, *33*, 2007293.
[5] D. I. Viswanath, H.-C. Liu, D. P. Huston, C. Y. X. Chua, A. Grattoni, *Biomaterials* **2022**, *280*, 121297.
[6] S. Jhunjhunwala, C. Hammer, L. Delamarre, *Nat. Rev. Cancer* **2021**, *21*, 298.
[7] F. Chen, Y. Wang, J. Gao, M. Saeed, T. Li, W. Wang, H. Yu, *Biomaterials* **2021**, *270*, 120709.
[8] D. H. Munn, V. Bronte, *Curr. Opin. Immunol.* **2016**, *39*, 1.
[9] S.-B. Yong, S. Ramishetti, M. Goldsmith, Y. Diesendruck, I. Hazan-Halevy, S. Chatterjee, G. Somu Naidu, A. Ezra, D. Peer, *Adv. Mater.* **2022**, *34*, 2106350.
[10] Y. Zhang, R. N. Sriramaneni, P. A. Clark, J. C. Jagodinsky, M. Ye, W. Jin, Y. Wang, A. Bates, C. P. Kerr, T. Le, R. Allawi, X. Wang, R. Xie, T. C. Havighurst, I. Chakravarty, A. L. Rakhmilevich, K. A. O'Leary, L. A. Schuler, P. M. Sondel, K. Kim, S. Gong, Z. S. Morris, *Nat. Commun.* **2022**, *13*, 4948.
[11] Y. Zhu, Z. Yang, Z. Pan, Y. Hao, C. Wang, Z. Dong, Q. Li, Y. Han, L. Tian, L. Feng, Z. Liu, *Sci. Adv.* **2022**, *8*, abo5285.
[12] Y. Guo, Y. Li, M. Zhang, R. Ma, Y. Wang, X. Weng, J. Zhang, Z. Zhang, X. Chen, W. Yang, *Nat. Commun.* **2024**, *15*, 8586.
[13] J. Sun, H. Yao, X. Ren, L. Cui, L. Liu, G. Wang, Z. Tang, *Nano Lett.* **2024**, *24*, 2921.
[14] X. Xu, T. Li, T. Yang, F. Liu, Z. Guo, H. Wu, Y. Tang, H. Chen, *Nano Lett.* **2024**, *24*, 12239.
[15] Z. Zhang, Z. Pan, Q. Li, Q. Huang, L. Shi, Y. Liu, *Sci. Adv.* **2024**, *10*, adk0716.
[16] Y. Huang, J. Zou, J. Huo, M. Zhang, Y. Yang, *Adv. Mater.* **2024**, *36*, 2407914.
[17] Y. Liu, L. Qiao, S. Zhang, G. Wan, B. Chen, P. Zhou, N. Zhang, Y. Wang, *Acta Biomater.* **2018**, *66*, 310.
[18] B. Pulendran, P. S. Arunachalam, D. T. O'Hagan, *Nat. Rev. Drug Discovery* **2021**, *20*, 454.
[19] Y. Zhang, L. Liu, H. He, Y. Sun, Z. Zhong, *Mater. Today* **2024**, *80*, 406.
[20] J. Zhao, Y. Xu, S. Ma, Y. Wang, Z. Huang, H. Qu, H. Yao, Y. Zhang, G. Wu, L. Huang, W. Song, Z. Tang, X. Chen, *Adv. Mater.* **2022**, *34*, 2109254.
[21] J. Han, T. Sheng, Y. Zhang, H. Cheng, J. Gao, J. Yu, Z. Gu, *Adv. Mater.* **2024**, *36*, 2209778.
[22] G. Cui, Y. Sun, L. Qu, C. Shen, Y. Sun, F. Meng, Y. Zheng, Z. Zhong, *Adv. Healthcare Mater.* **2024**, *13*, 2303690.
[23] F. Chen, T. Li, H. Zhang, M. Saeed, X. Liu, L. Huang, X. Wang, J. Gao, B. Hou, Y. Lai, C. Ding, Z. Xu, Z. Xie, M. Luo, H. Yu, *Adv. Mater.* **2023**, *35*, 2209910.
[24] E. N. Chin, A. Sulpizio, L. L. Lairson, *Trends Cell Biol.* **2023**, *33*, 189.
[25] R. Endo, T. Ueda, T. Nagaoki, N. Shima, Y. Sato, H. Harashima, T. Nakamura, *J. Controlled Release* **2024**, *372*, 609.
[26] S. Van Herck, B. Feng, L. Tang, *Adv. Drug Delivery Rev.* **2021**, *179*, 114020.
[27] J. Yang, Z. Luo, J. Ma, Y. Wang, N. Cheng, *J. Controlled Release* **2024**, *371*, 273.
[28] X. Shi, L. Shu, M. Wang, J. Yao, Q. Yao, S. Bian, X. Chen, J. Wan, F. Zhang, S. Zheng, H. Wang, *Adv. Sci.* **2023**, *10*, 2204890.
[29] T. Su, Y. Zhang, K. Valerie, X.-Y. Wang, S. Lin, G. Zhu, *Theranostics* **2019**, *9*, 7759.
[30] J. Guo, J. Huang, Z. Huang, D. Hu, H. Tan, Y. Wang, C. Deng, X. Zhu, Z. Zhong, *Nat. Commun.* **2025**, *16*, 6239.
[31] Z. Zhu, T. Chen, F. Huang, S. Wang, P. Zhu, R. X. Xu, T. Si, *Adv. Mater.* **2024**, *36*, 2304840.
[32] Z. Luo, Y. Wang, J. Li, J. Wang, Y. Yu, Y. Zhao, *Adv. Funct. Mater.* **2023**, *33*, 2306554.
[33] J. Guo, H. Tan, W. Chen, Y. Wang, W. Lin, Z. Zhong, C. Deng, *J. Controlled Release* **2025**, *385*, 114003.
[34] B. L. Nguyen, C. D. Phung, D.-V. Pham, N. D. Le, T. O. O. Nguyen, S. Kim, S. G. Jin, H.-G. Choi, J.-H. Chang, C. H. Song, J. Kim, S. K. Ku, J. O. Kim, *Nano Today* **2024**, *55*, 102179.
[35] Y. Xia, J. Wei, S. Zhao, B. Guo, F. Meng, B. Klumperman, Z. Zhong, *J. Controlled Release* **2021**, *336*, 262.
[36] J. Li, P. Zhang, M. Zhou, C. Liu, Y. Huang, L. Li, *ACS Nano* **2022**, *16*, 6064.
[37] J. M. Ramanjulu, G. S. Pesiridis, J. Yang, N. Concha, R. Singhaus, S.-Y. Zhang, J.-L. Tran, P. Moore, S. Lehmann, H. C. Eberl, M. Muelbaier, J. L. Schneck, J. Clemens, M. Adam, J. Mehlmann, J. Romano, A. Morales, J. Kang, L. Leister, T. L. Graybill, A. K. Charnley, G. Ye, N. Nevins, K. Behnia, A. I. Wolf, V. Kasparcova, K. Nurse, L. Wang, A. C. Puhl, Y. Li, et al., *Nature* **2018**, *564*, 439.
[38] X. W. Shi, L. W. Shu, M. W. Wang, J. Yao, Q. G. Yao, S. C. Bian, X. N. Chen, J. Q. Wan, F. Zhang, S. S. Zheng, H. X. Wang, *Adv. Sci.* **2023**, *10*, 2204890.
[39] W. Ma, R. Sun, L. G. Tang, Z. B. Li, L. Lin, Z. Y. Mai, G. Chen, Z. Q. Yu, *Adv. Mater.* **2023**, *35*, 2303149.
[40] Y. Li, K. Deng, C. Shen, X. Liang, Z. Zeng, L. Liu, X. Xu, *ACS Nano* **2023**, *17*, 17320.
[41] H. Liu, W. Shen, W. Liu, Z. Yang, D. Yin, C. Xiao, *Bioact. Mater.* **2024**, *31*, 206.
[42] Z. Deng, M. Xi, C. Zhang, X. Wu, Q. Li, C. Wang, H. Fang, G. Sun, Y. Zhang, G. Yang, Z. Liu, *ACS Nano* **2023**, *17*, 4495.
[43] Z. Li, X. Lai, S. Fu, L. Ren, H. Cai, H. Zhang, Z. Gu, X. Ma, K. Luo, *Adv. Sci.* **2022**, *9*, 2201734.
[44] H. Xiao, X. Li, S. Liang, S. Yang, S. Han, J. Huang, X. Shuai, J. Ren, *ACS Nano* **2024**, *18*, 11070.
[45] Z. Liu, J. Zhang, H. Liu, H. Shen, N. Meng, X. Qi, K. Ding, J. Song, R. Fu, D. Ding, G. Feng, *Adv. Mater.* **2023**, *35*, 2208692.
[46] M. He, M. Zhang, T. Xu, S. Xue, D. Li, Y. Zhao, F. Zhi, D. Ding, *J. Controlled Release* **2024**, *368*, 233.
[47] Y. Wu, J.-Y. Lin, Y.-D. Zhou, H.-J. Liu, S.-X. Lu, X.-K. Zhang, Y.-Y. Guan, D. G. Nagle, W.-D. Zhang, H.-Z. Chen, X. Luan, *Adv. Healthcare Mater.* **2024**, *13*, 2303445.
[48] H. Xiao, X. Li, B. Li, S. Yang, J. Qin, S. Han, J. Ren, X. Shuai, *Small* **2023**, *19*, 2300280.
[49] G. Chen, Y. Wang, L. Mo, X. Xu, X. Zhang, S. Yang, R. Huang, R. Li, L. Zhang, B. Zhang, *ACS Nano* **2024**, *18*, 20296.
[50] B. C. Taylor, X. Sun, P. I. Gonzalez-Ericsson, V. Sanchez, M. E. Sanders, E. C. Wescott, S. R. Opalenik, A. Hanna, S.-T. Chou, L. Van Kaer, H. Gomez, C. Isaacs, T. J. Ballinger, C. A. Santa-Maria, P. D.

Shah, E. C. Dees, B. D. Lehmann, V. G. Abramson, J. A. Pietenpol, J. M. Balko, *Cancer Discovery* **2024**, *14*, 290.
[51] J. Jiang, M. Zhang, T. Lyu, L. Chen, M. Wu, R. Li, H. Li, X. Wang, X. Jiang, X. Zhen, *Adv. Mater.* **2023**, *35*, 2300854.
[52] C. Zhong, J. Li, S. Liu, W. Li, Q. Zhang, J. Zhao, M. Xiong, Y. Bao, Y. Yao, *Theranostics* **2023**, *13*, 2800.
[53] Y. He, C. Hong, S. Huang, J. A. Kaskow, G. Covarrubias, I. S. Pires, J. C. Sacane, P. T. Hammond, A. M. Belcher, *Adv. Healthcare Mater.* **2023**, *12*, 2300688.
[54] W. J. Jin, J. C. Jagodinsky, J. M. Vera, P. A. Clark, C. L. Zuleger, A. K. Erbe, I. M. Ong, T. Le, K. Tetreault, T. Berg, A. L. Rakhmilevich, K. Kim, M. A. Newton, M. R. Albertini, P. M. Sondel, Z. S. Morris, *Cell Rep.* **2023**, *42*, 113556.
[55] P. Zhang, T. Wang, G. Cui, R. Ye, W. Wan, T. Liu, Y. Zheng, Z. Zhong, *Adv. Mater.* **2024**, *36*, 2407189.
[56] S. Fu, Y. Li, L. Shen, Y. Chen, J. Lu, Y. Ran, Y. Zhao, H. Tang, L. Tan, Q. Lin, Y. Hao, *Small* **2024**, *20*, 2309537.
[57] A. Som, J.-G. Rosenboom, A. Chandler, R. A. Sheth, E. Wehrenberg-Klee, *Adv. Drug Delivery Rev.* **2022**, *189*, 114505.
[58] L. Qu, G. Cui, Y. Sun, R. Ye, Y. Sun, F. Meng, S. Wang, Z. Zhong, *Adv. Mater.* **2024**, *36*, 2409590.
[59] M. Gouez, A. Rébillard, A. Thomas, S. Beaumel, E.-L. Matera, E. Gouraud, L. Orfila, B. Martin, O. Pérol, C. Chaveroux, E. N. Chirico, C. Dumontet, B. Fervers, V. Pialoux, *Front. Immunol.* **2024**, *15*, 1368550.
[60] J.-H. Kim, S.-Y. Park, S.-E. Jeon, J.-H. Choi, C.-J. Lee, T.-Y. Jang, H.-J. Yun, Y. Lee, P. Kim, S. H. Cho, J. S. Lee, J.-S. Nam, *Theranostics* **2022**, *12*, 5258.